Matrix-assisted laser desorption/ionization mass spectrometry imaging for the analysis of pro-and anti-inflammatory macrophages and murine and human atherosclerotic tissue samples

Cumulative dissertation

Presented by

Pegah Khamehgir-Silz

Submitted to the

Faculty of Biology and Chemistry

and prepared at the

Institute of Inorganic and Analytical Chemistry

For the degree of

Doctor rerum naturalium (Dr. rer. nat.)

Justus Liebig University Giessen, Germany

Giessen 2025

This thesis was accepted as a doctoral dissertation in fulfilment of the requirements for the degree of Doctor Rerum Naturalium by the Faculty of Biology and Chemistry, Justus-Liebig-University Giessen, Germany.

1. Referee: Prof. Dr. Bernhard Spengler
2. Referee: Prof. Dr. Andreas H. Wagner

Content

List of Publication

This thesis is based on the following publications in peer-reviewed journals;

1. Pegah Khamehgir-Silz, Florian Schnitter, Andreas H. Wagner, Stefanie Gerbig, Sabine Schulz, Markus Hecker and Bernhard Spengler, Strategy for marker-based differentiation of pro- and anti-inflammatory macrophages using matrix-assisted laser desorption/ionization mass spectrometry imaging, Analyst, 2018,143, 4273-4282

2. Pegah Khamehgir-Silz, Stefanie Gerbig, Nadine Volk, Sabine Schulz, Bernhard Spengler, Markus Hecker, Andreas H. Wagner, Comparative lipid profiling of murine and human atherosclerotic plaques using high-resolution MALDI MSI, Pflugers Arch. 2022; 474(2): 231–242.

List of Abbreviations

MALDI	Matrix-assisted laser desorption ionization
MSI	Mass spectrometry imaging
FFPE	Formalin fixed paraffin embedded
AP	Atmospheric pressure
ROI	Region of interest
TIC	Total ion count
H&E	Hematoxylin and eosin
PCA	Principal component analysis
HCA	Hierarchical clustering analysis
ANOVA	Analysis of variance
qPCR	Quantitative Polymerase chain reaction
FACS	Fluorescence-activated cell sorting
FCS	Fetal calf serum
M-CSF	Macrophage FCS
LPS	Lipopolysaccharide
CVD	Cardiovascular diseases
Ox-LDL	Oxidized low-density lipoprotein
CD	Cluster of differentiation
LC-MS	Liquid chromatography-mass spectrometry
MRM	Multiple reaction monitoring
ApoE	Apolipoprotein E
CE	Cholesterol esters
LPC	Lysophosphatidylcholines
LPE	Lysophosphatidylethanolamines
CED	Cholesterol ester derivatives
BCA	Brachiocephalic artery

Zusammenfassung

Diese Dissertation beschäftigt sich mit der Anwendung von Matrix-unterstützter Laser-Desorption/Ionisierung Massenspektrometrie-Imaging (MALDI-MSI) zur Visualisierung und Charakterisierung von proinflammatorischen und antiinflammatorischen Makrophagen sowie atherosklerotischen Plaques in murinen Modellen und humanen Gewebeproben.

Eine umfassende Methodik zur Unterscheidung proinflammatorischer und antiinflammatorischer humaner Makrophagen anhand von MALDI-MSI, RT-qPCR und FACS wurde in der erstem Publikation erarbeitet. Mittels RT-qPCR und FACS konnten die Makrophagen-Subtypen M1, M2a und M2c anhand von Expressionsprofilen markierter Gene erfolgreich unterschieden werden. Ein umfassender Arbeitsablauf für die Probenpräparation, Messung und Datenanalyse mittels MALDI-MSI wurde erarbeitet und etabliert. Die etablierte Methode zeigte eine gute Reproduzierbarkeit in drei biologischen Replikaten. Basierend auf einer Hauptkomponentenanalyse (PCA) und einer hierarchischen Clusteranalyse (HCA) konnten subtypspezifische Marker identifiziert werden. Allerdings zeigte sich bei der Erhöhung der biologischen Replikate die Heterogenität von Zellen verschiedener Spender. Diese biologische Variabilität stellte eine Herausforderung bei der Identifizierung universeller Marker in in-vitro stimulierten humanen Makrophagen dar.

In der zweiten Studie wurden Lipidmarker, die mit der Plaquebildung und -entwicklung bei ApoE-/- Mäusen in Verbindung stehen, erfolgreich identifiziert und deren Präsenz in humanem atherosklerotischem Gewebe untersucht. Insgesamt wurden 31 Verbindungen ausschließlich in ApoE-/- Mäusen detektiert und somit als Marker identifiziert. Die stark voneinander abweichenden Lipidprofile der humanen Gewebeproben ließen die Detektion und Identifikation von universellen Markern nicht zu. In einigen humanen Gewebeproben konnten Überschneidungen zu den in den murinen Gewebeproben detektierten Markern festgestellt werden. Diese Ergebnisse unterstreichen die biologische Variabilität von humanen Proben und zeigen ein patientenabhängiges Lipidprofil. Dies wird durch frühere Forschungsergebnisse, die darauf hinweisen, dass klinisch relevante atherosklerotische Plaques eine variable Mischung von Lipiden enthalten, untermauert. Die in dieser Untersuchung festgestellten Unterschiede in den Lipidprofilen humaner Gewebeproben lassen sich auf verschiedene Stadien der Atherosklerose sowie Faktoren wie Ernährung, Lebensgewohnheiten und die Einnahme cholesterinsenkender Medikamente zurückführen. Die Notwendigkeit individuelle Patientenmerkmale bei der Untersuchung atheroskletorischer Plaques zu berücksichtigen, wird durch diese Forschungsergebnisse nochmals untermauert.

Diese Arbeit liefert einen wichtigen Beitrag zum Verständnis der Lipid-zusammensetzung im Kontext von Atherosklerose und unterstreicht das Potenzial von MALDI-MSI als leistungsfähige Methode zur Untersuchung von Makrophagen und Plaques in murinen Modellen und humanen Proben. Die durch diese Dissertation gewonnenen Erkenntnisse bilden eine wertvolle Basis für zukünftige Forschungs-projekte und könnten dabei helfen, neue diagnostische und therapeutische Ansätze für Herz-Kreislauf-Erkrankungen zu entwickeln.

Abstract

The primary objective of this dissertation is the use of Matrix-Assisted Laser Desorption/Ionization Mass Spectrometry Imaging (MALDI MSI) for the visualization and characterization of pro- and anti-inflammatory macrophages as well as atherosclerotic plaques in murine models and human tissue samples.

In the first publication, a comprehensive methodology was developed to distinguish pro- and anti-inflammatory human macrophages using MALDI-MSI, RT-qPCR, and FACS. The macrophage subtypes M1, M2a, and M2c could be successfully distinguished based on expression profiles of marker genes using RT-qPCR and FACS. A comprehensive working protocol for the preparation, measurement and data analysis for MALDI-MSI was developed and established. The method identified subtype-specific markers and showed good reproducibility in three biological replicates based on principal component analysis (PCA) and hierarchical cluster analysis (HCA). The heterogeneity of cells from different donors became apparent when the number of biological replicates was increased from 3 to 6. Due to the biological variability of cells derived from various donors, identifying universal markers for in-vitro stimulated human macrophages posed challenges.

In the second publication, lipid markers associated with plaque formation and development in ApoE-/- mice were successfully identified, and their presence in human atherosclerotic tissue was investigated. The determined results clearly showed differences in the lipid profile of the older ApoE-/-mice compared to the wild-type mice. Thirty-one compounds that were exclusively detected in the ApoE-/- mice were identified as markers. The results of the human atherosclerotic tissue samples showed significantly different lipid profiles, making it difficult to identify universal markers. However, in particular tissue samples, it was possible to detect markers identified in the murine plaques tissue samples. These findings demonstrate a patient-specific lipid profile and support previous findings suggesting that clinically significant atherosclerotic plaques contain a variable mixture of lipids. The detected variance in lipid compositions could be related to different stages of atherosclerosis progression and factors such as diet, lifestyle and medication. These findings highlight the necessity of considering unique patient characteristics, such as medication history, when analyzing lipid profiles in atherosclerosis studies.

Overall, this PhD thesis contributes to our understanding of the lipid composition in atherosclerotic plaques and highlights the potential of MALDI MSI as a valuable, powerful technique for studying macrophages and atherosclerotic plaques in murine models and human samples. The findings provide a useful basis for future research approaches and may aid in developing novel diagnostic and therapeutic strategies for cardiovascular disease.

1. Summary

1.1 Introduction

Atherosclerosis is a complex and multifaceted chronic inflammatory disease primarily affecting medium- and large-sized arteries. It is one of the most common causes of cardiovascular diseases and a major risk factor for heart attacks and strokes, occurring when fats, cholesterol and other substances accumulate on the inner walls of arteries, narrowing or blocking them. According to the World Health Organization (WHO), cardiovascular diseases are the world's leading cause of death, responsible for over 17,9 million deaths in 2019, representing 32% of all global deaths. 85% of these deaths were due to heart attack and stroke[1]. Understanding the mechanism of coronary atherosclerotic plaque formation is crucial for preventing and treating atherosclerosis. Reducing the number of heart attacks and strokes is of utmost importance.

Inflammation plays a major role in the progression of atherosclerosis, with monocytes and macrophages being the primary immune cells involved[2]. Monocytes originate in the bone marrow from pluripotent stem cells. They are recruited to the sites of injury or pathogen invasion, adhere to endothelial cells, enter the subendothelial space and differentiate into lesional macrophages[3,4]. The recruitment and transmigration of monocytes is due to endothelial dysfunction and activation, which refers to a decrease in the production and activity of nitric oxide by endothelial cells[5]. This dysfunction can be caused by factors such as oxidative stress, high cholesterol, diabetes, and hypertension and is characterized by the expression of adhesion molecules on the surface of endothelial cells[6], which allows circulating leukocytes to attach to the vessel wall[7–9]. In the early stages of atherosclerosis, macrophages accumulate within the subendothelium or neointima. Chemokines recruit additional monocytes if the arterial insult persists[10,11]. The macrophages ingest modified lipids and other substances that accumulate in the subendothelium, forming fatty streak lesions[12]. The growth of fatty streaks or pathological intimal thickening with macrophages primarily occurs by getting more macrophages and expanding macrophage foam cells[11].

Macrophages are cells with remarkable plasticity, allowing them to switch between promoting or suppressing inflammation. Classically, macrophages have been classified into two phenotypes, M1 and M2. M1 macrophages are *in vitro* induced by interferon-γ and the toll-like receptor four ligand lipopolysaccharide and promote inflammation by producing pro-inflammatory cytokines, chemokines, and reactive oxygen species. A subset of alternatively *in vitro* activated macrophages, M2 macrophages, can be induced by IL-4 (M2a), IL-10 (M2c) and IL-13 and promote tissue repair and remodeling by producing pro-resolving molecules[13]. There are also other macrophage populations, e.g. Mox, Mhem, and M4, which are suggested to be present in atherosclerotic lesions [14,15]. The phenotype of lesional macrophages cannot be classified into predefined subsets but is instead a consequence of the lesional microenvironment, which is highly dependent on systemic factors, e.g. dyslipidemia[16,17] and/or diabetes mellitus[18] and the activation of specific intracellular signaling pathways. Lesional macrophages can rapidly change their phenotype in response to changes in the microenvironment and signaling pathways, making it best to view them as representing a comprehensive continuum of phenotypes and functions[11].

There are various markers used for the immunohistochemical staining of for example M1[19–22] (iNOS, CD80, CD86, TNF-alpha, IL-12, IL-6, IL-1beta, CXCL9, CXCL10), M2a[20,23,24] (CD206, Arginase-1, CD163 and IL-10), and M2c[13,14] (CD163, CD206, CD14, TGF-beta, and IL-10) macrophages. The aboved mentioned markers are crucial in identifying and characterizing these distinct macrophage subtypes in tissue samples. One challenge in using immunohistochemistry for the identification of macrophage subtypes is that some markers, such as CD163 and CD206, can be expressed in multiple macrophage subtypes, including M2a and M2c. This lack of absolute specificity can make it challenging to identify the different subtypes definitively in immunohistochemistry studies. Furthermore, this is not only a challenge for macrophage characterization but a general problem in the discovery of biomarkers.

Hulka et al.[25] define biomarkers as "cellular, biochemical, or molecular alterations that are measurable in biological media such as human tissues, cells, or fluids." One of the most recent additions is "a defined characteristic that is measured as an indicator of normal biological processes, pathogenic processes, or responses to an exposure or intervention[26]." Biological molecules, which include any gene, protein, or metabolite, are known as biomarkers. They are employed in the identification, diagnosis, and surveillance of illnesses in addition to forecasting therapeutic or clinical results. Biomarkers may aid in developing tailored treatments, offer precise and timely diagnosis, and shed light on the prognosis of certain diseases[27]. Numerous restrictions and analytical difficulties affect the validity, repeatability, and practicality of biomarker identification in clinical settings. Biological variability is a major obstacle in the identification of biomarkers. Although biomarkers need to be dependable and consistent across populations and individuals, biomarker expression can vary significantly due to genetic diversity, varying backgrounds, and varying degrees of personal care[28]. As a result, samples from people with the same nominal disease exhibit significant variability. Protein expression can also be strongly influenced by lifestyle, dietary and treatment plans. One example of this is the breast proliferation index, which is influenced by oral contraceptives[29]. The identification of universally applicable biomarkers is made more difficult by this variability. Analytical sensitivity and specificity are important additional considerations. For the measurement of biomarkers to accurately detect low concentrations in biological samples, very sensitive and specific methods are needed. Molecules must be precisely distinguished from one another which is frequently difficult by structural similarities. There is a big challenge with these technical requirements. In atherosclerosis, markers are employed to characterize and distinguish these various macrophage subtypes, depending on the context of in vivo and/or in vitro. However, this approach has led to confusion regarding the identity and features of these distinct macrophage subtypes because there are no established and accepted guidelines for their classification.

Moreover, macrophages in tissue samples can be heterogeneous, with different activation states and phenotypes, which make the precise identification more complicated. Immunohistochemistry provides valuable information about the presence and distribution of macrophage subtypes in tissues with limitations in revealing cellular function and cytokine release. To address these limitations, researchers often employ different techniques, including immunohistochemistry, gene expression analysis and functional assays to comprehensively characterize macrophage populations in tissues.

A robust method for measuring metabolites and identifying known and unknown chemicals in biological samples is liquid chromatography (LC)–mass spectrometry (MS). This approach is used for e.g. determining drug toxicity[30] and identifying biomarkers for disease diagnosis[31]. By monitoring changes in signaling molecules, investigating how immune cells and immunological responses work can be employed[32,33]. The study of Zhang et al.[34] explored the dynamic lipid profiles associated with different macrophage stages using targeted LC-MS with multiple reaction monitoring (MRM). This technique enables the detection of a wide range of lipid compounds simultaneously. Zhang et al. could identify over 300 distinct lipid molecules in mammalian macrophages. The main lipid classes identified in this study belong to the following groups: phosphatidylcholine (PC), phosphatidylserine (PS), phosphatidylethanolamine (PE), phosphatidylinositol (PI), phosphatidylglycerol (PG), sphingomyelin (SM), and ceramide (Cer). Additionally, the researchers detected a shift in glycerolipids (GLs) composition from short-chain saturated and monounsaturated lipids to long-chain polyunsaturated lipids in the activated human macrophages derived from THP-1 cells. Compared to M1 macrophages in mice, M2 macrophages showed higher levels of lysoGLs. They also show that IL-4-induced M2 macrophages, derived from human and mouse monocytes, had significantly increased in the levels of lysoPI during polarization. These findings show a dynamic shift in the lipid composition when monocytes differentiate into macrophages, offering further insight into the processes of macrophage differentiation and polarization. This lipid-focused study has potential for identifying new markers of inflammation.

In another study, Abuawad et al.[33] used untargeted LC-MS-based metabolite profiling to characterize M1 and M2 macrophages derived from THP-1 cells to identify the key characteristic metabolites of each polarization state. The data show a clear metabolic signatures and corresponding metabolite changes associated with M1 and M2 phenotypes. The study employed an Acela system connected to an Exactive MS (Thermo Fisher Scientific) operating in both negative (ESI−) and positive (ESI+) ion modes for LC-MS-based metabolite profiling. The polarized M1 and M2 macrophages were distinguished from the unpolarized THP-1 macrophages (M0) by analyzing the surface markers and the cytokine profiles. Thereby, Abuawad et al. identified significant differences between the unpolarized and polarized groups, with M1 macrophages showing higher levels of the pro-inflammatory cytokines TNF-α and IL-1β than M2 and M0 macrophages. Intracellular metabolites were extracted from the different macrophage types and analyzed, showing that the metabolome consisted primarily of glycerophospholipids (20%), amino acids (17%), fatty acyls (7%), lipids (6%), carbohydrates (5%), nucleotides (3%), sphingolipids (3%), co-factors and vitamins (2%) and energy metabolites (1%). In total, Abuawad et al. were able to identify 644 metabolites presumptively. The researcher show that the technique was sensitive enough to distinguish small metabolite changes due to macrophage polarization, thereby identifying metabolic signatures for M1 and M2 phenotypes. The study highlighted various metabolic pathways significantly altered in these macrophage types. These results provide new insights into macrophage polarization mechanisms and suggest new strategies for developing immune-modulatory approaches.

Besides liquid chromatography (LC)–mass spectrometry, there are also other powerful techniques for cell analysis. Strittmatter et al.[35], for example, use the rapid evaporative ionization mass spectrometry (REIMS) methodology to characterize and identify intact bacterial cells by subjecting them to a radiofrequency (RF) electrical current for the first time. The mass spectrometric analysis was directly performed from an agar plate, with bacterial biomass collected from the solid growth medium by using forceps electrodes. The biomass was rapidly heated, and the aerosol containing gas-phase ions of metabolites and structural lipids was directly introduced into a mass spectrometer for online chemical analysis. In the investigation, mass spectrometric analysis was employed to detect nine distinct bacterial species from eight different genera and four different bacterial families, totaling ninety separate clinical isolates. Using a verified database, a species-level identification was possible by substantially less intra-species variance than inter-species variance. Pre-processing of the spectral dataset was done to consider the bio-analytical complexity of mass spectrometric profiles. Using unsupervised principal components analysis (PCA), spectral differences and similarities between samples were analyzed. Molecular ion patterns unique to each species were extracted using the Maximum Margin Criterion Analysis (MMC). This approach identified Gram-positive Streptococcus species, Staphylococcus aureus, Gram-negative Pseudomonas aeruginosa, and five unrelated Enterobacteriaceae species as four distinct clusters. The investigation showed that the REIMS method is a feasible approach for species-level clinical isolate identification.

In a recently published research paper, Eroles et al.[36] combined atomic force microscopy (AFM) high-resolution viscoelastic mapping with interference contrast microscopy (ICM) at the single-cell level to investigate monocytes and macrophages. The study aimed to investigate the changes in cell mechanics and adhesion of monocytes and differentiated macrophages during monocyte differentiation into macrophages. By using the described approach, the researcher could demonstrate that macrophages have a greater adhesion area and decreased cellular fluidity. Adhesion to surfaces via a reinforcing mechanism may cause these mechanical changes. Interestingly, spread macrophages were almost three times more rigid than their round counterparts. However, this correlation was not apparent when analyzing average values for spread macrophages. The results indicate a major biological significance for stiffening, solidification and size expansion processes when monocytes differentiate into macrophages. Larger, more rigid, and more solidly packed macrophages may be more adept at carrying out mechanosensitive functions like phagocytosis and migration.

In addition to the methods mentioned above, mass spectrometry imaging (MSI) is another powerful technique for identifying and characterizing cells and tissue samples. This technique is allowing researchers to visualize the spatial distribution of various molecules within tissue sections[37]. Over 50 years ago, MSI was described for the first time by Andersen et al. by introducing secondary ion mass spectrometry (SIMS)[38]. Since then, several MSI techniques, e.g. MALDI MSI[39–42], (nano)DESI[43,44], LAESI[45], LA-ICP-MS[46] were developed with specific benefits and limitations[47]. In Figure 1, some MSI techniques, including spatial resolution and sensitivity, are shown.

MSI experiments aim to assess the spatial distribution of molecules[48] quantitatively. Nonetheless, factors such as ionization efficiency, ion suppression, and matrix effects

resulting from sample heterogeneity constrain the precision of laser-based MSI techniques. Matrix effects often arise in MSI investigations[49,50]; however, the extent of signal suppression depends on the analyt/matrix composition. The variations in the chemical composition of species obtained from different anatomical regions of various tissue slices are the main factor affecting the extent of matrix effects seen in tissue imaging. In various scanning imaging tests, two types of matrix effects have been observed: (a) ionization suppression due to the competition among molecules for charge, and (b) signal enhancement or suppression affected by variations in alkali metal concentrations across different tissue sample locations[49,51,52]. The impact of matrix effects, regardless of their origin, can modify the spatial distribution of molecules impacting the measurement of these substances across various regions of the tissue sample. For accurate measurements in QMSI studies, it is essential to compensate for matrix effects. A range of normalization strategies has been developed to address matrix effects in mass spectrometry imaging (MSI), with the normalization of ion signals to the total ion count (TIC) being the most commonly used approach.

Nonetheless, this approach maintains the signal variations caused by matrix effects, as demonstrated in studies by Lanekoff et al.[49] using a middle cerebral artery occlusion (MCAO) stroke model in murine subjects. The experiment involved the execution of nanoDESI MSI utilizing a solvent that contained two phosphatidylcholine (PC) standards, specifically PC 25:0 and PC 43:6. The findings indicated an uneven distribution of sodium and potassium adduct signals, suggesting that matrix effects were influenced by ischemia and the increased concentrations of glycolipids identified in brain tissue. The results underscore the constraints associated with TIC normalization. Alternatively, the normalization process to the standard has demonstrated efficacy in producing ion images devoid of matrix effects, as it entails adjusting endogenous PC signals to align with the corresponding adduct of the PC standard. This approach demonstrates the potential for precisely measuring concentration gradients in tissue samples. It facilitates the application of various standards to evaluate matrix influences across different lipid and metabolite categories in mass spectrometry imaging experiments[53].

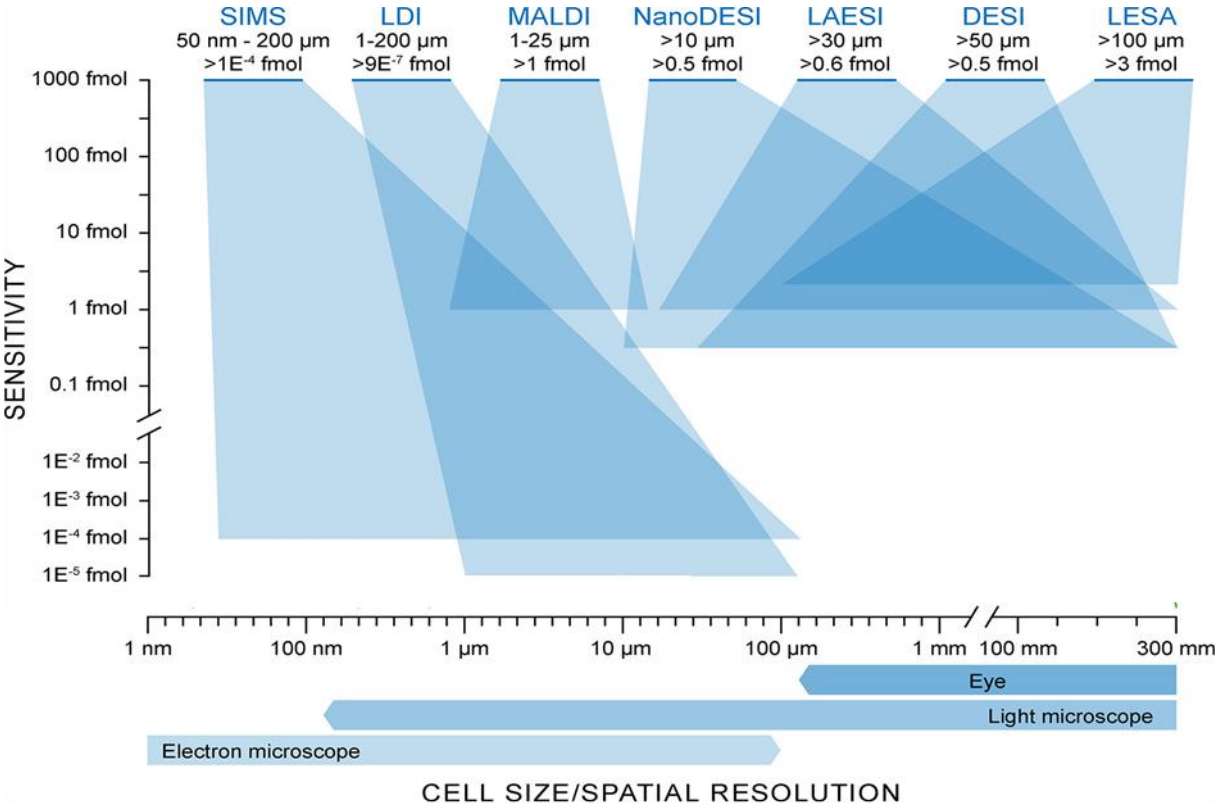

Figure 1: Commonly used MSI techniques for investigating metabolomics and proteomics. This figure was taken and adapted from the paper published by Tylor et al.[54]

As mentioned aboved matrix-assisted laser desorption/ionisation mass spectrometry imaging (MALDI MSI) has become the most widely used technicque for the visualisation and investigation of several molecular groups[55–62] within biological systems[37,40,63–65]. MALDI was introduced in the 1980s by F. Hillenkamp and M. Karas[42] as a soft ionisation technique that allows analysing intact biomolecules. B. Spengler further developed MALDI to MALDI MSI in 1994, including information about the spatial distribution of biomolecules[40]. This approach was subsequently developed and applied to tissue section analysis[64,66,67].

The principle workflow of a MALDI MSI experiment is shown in Figure 2[59]. At first, a thin tissue section (mostly fresh frozen or FFPE[68,69]) is covered by a matrix. The matrix choice and sample preparation protocol are crucial for the experiment's success. In the second step, a laser ablates a thin matrix layer with intense laser pulses over a short duration. Rapid heating leads to the matrix's expansion and intact analyte molecules into the gas phase (matrix plume), promoting ionization in the process[70,71]. The laser is raster-scanning the sample pixel by pixel with a fixed step size. For each pixel, a mass spectrum is recorded, which can be reconstructed through specific MSI software[72–74] to MS images showing the spatial distribution of hundreds of unknown compounds in a single measurement with lateral resolutions down to 1.4 µm[75]. By using databases[76–78], molecule annotation can be made, benefitting from high mass accuracy (< 2 µm) and a high mass resolution for a reliable assignment.

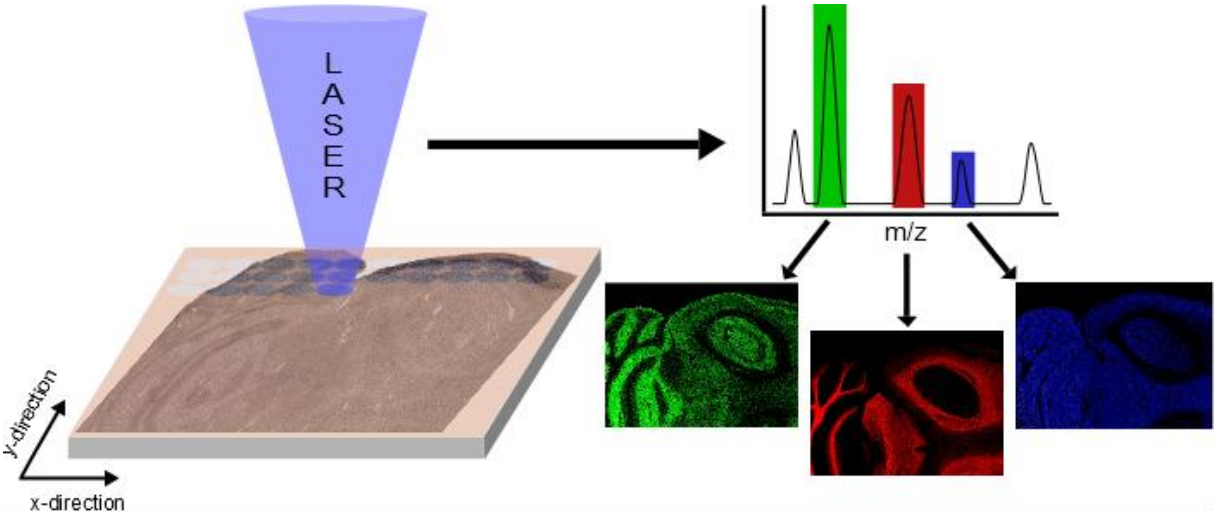

Figure 2: Scheme of a mass spectrometry imaging experiment. A tissue section covered by a matrix is scanned/irradiated by a pulsed laser. A mass spectrum is recorded for each pixel, and MS images are generated for the whole tissue for different m/t peaks.

This label-free and non-targeted[79] method allows histological tissue examination after the MALDI MSI measurement in the same tissue section[80].

The aforementioned lateral resolution of 1.4 µm was developed only in the last decade and enables the laterally resolved analysis of intact biomolecules in even smaller samples than before. The research paper of Müller et al.[81] uses atmospheric-pressure scanning microprobe matrix-assisted desorption/ionization mass spectrometry imaging (AP-SMALDI) in positive and negative ion mode with a pixel size down to a cellular level (1,5 µm) to examine, the lipidomic phenotypes of human naïve and activated microglia-like cells (MGLCs). Microglia are non-neuronal cells of the central nervous system which play a crucial role in homeostasis, cellular upkeep, and brain development[82–85]. By analyzing the lipid contents of individual cells on biological triplicates, the researchers were able to visualize population-based and single-cell-based heterogeneities in MGLCs. The work shows how individual cells within the same cell culture can differ from one another both intra- (e.g. LD´s) and inter-cellular (e.g. PI´s), suggesting that MGLCs have undergone phenotypic differentiation. The researchers detected and visualized sub-cellular inflammation-induced heterogeneity generated throughout lipid droplet formation by MSI. The study demonstrated that single-cell heterogeneity, especially in negative-ion mode, affect the entire cell body despite cell line and stimulation. LPS activates the inflammatory response of microgliar resulting in a higher heterogeneity compared to samples not treated with LPS. This outcome shows that lipidomic phenotypes of single cells in culture can be distinguished using modern MSI technologies. The result highlights the need for further comprehensive studies to determine cellular lipidome heterogeneity or sub-cellular components' heterogeneity.

Recent studies in the field of atherosclerosis have employed MALDI MSI as a novel strategy to visualize atherosclerotic plaques. In the study of Cao et al. [86], 2D and 3D MALDI MSI was used to identify and verify aortic plaque-specific lipids common in high-fat-diet-fed low-density lipoprotein receptor-deficient (ldlr–/–) mice and chow-fed apolipoprotein E deficient (apoe–/–) mice. In both mouse models, 11 lipids were identified. Especially, lysolipids including lysophosphatidic acids,

lysophosphatidylcholines, lysophosphatidylethanolamines, lysophosphatidylinositols and sphingomyelins have been identified as being distinctly and significantly co-localized with the plaques. Among these, certain lysolipids and SM 34:0;2 were found to be characteristic for atherosclerotic plaques in the aorta, while LPI 18:0 was primarily concentrated in the necrotic core of the plaque.

In another study, Visscher et al.[87] developed a protocol utilizing MALDI MSI to explore the lipid composition of advanced human carotid plaques. The researchers studied three samples: two from endarterectomies representing advanced plaques and one from an autopsy representing an early-stage plaque. Their analysis revealed that diacylglycerols were more prevalent in thrombotic regions, and they could differentiate between advanced and early-stage plaques by assessing the cholesteryl ester profiles. The researcher aims to apply this method to a more extensive collection of carotid atherosclerotic plaque samples in future studies.

The study of Mörman et al.[88] aimed to investigate the spatial distribution of lipids in human carotid atherosclerotic plaque tissue samples and investigate the relation between lipids and compositional features of plaque vulnerability using MALDI MSI in positive-ion mode. A large dataset of a series of human plaques was collected and investigated. The researcher showed that certain sphingomyelins (SM) and oxidized cholesterol esters (oxCE) are significantly more expressed in the necrotic core (NC) region. Additionally, Mörmann et al. detected a correlation between diacylglycerol (DG´s) and triacylglycerol (TGs) and thrombus fragments, which could be used as possible markers for intraplaque bleeding.

In recent years, many research papers using MALDI MSI to investigate atherosclerosis have been published, resulting in the identification of various lipid markers that contribute to a deeper understanding of the causes and underlying mechanisms of plaque formation and progression[89–94].

1.2 Strategy for marker-based differentiation of pro- and anti-inflammatory macrophages using matrix-assisted laser desorption/ionization mass spectrometry imaging – (Publication 1 of the cumulative dissertation)[95]

This paper introduces a detailed methodology for distinguishing pro-inflammatory and anti-inflammatory human macrophages using matrix-assisted laser desorption/ionization mass spectrometry imaging (MALDI-MSI) in combination with real-time quantitative PCR (RT-qPCR) and fluorescence-activated cell sorting (FACS). A widely accepted protocol for differentiating human monocytes into macrophage subtypes M1 (INF-γ), M2a (IL-4) and M2c (IL-10) was employed. Using appropriate cytokine combinations, a monocyte purity of up to 94% was achieved and successfully differentiated in vitro. The macrophage subtypes were distinguished based on their gene expression profiles at the mRNA as well as the protein levels and the results demonstrated a correlation between mRNA levels and protein abundance. Notably, the M2c subtype stimulus IL-10 led to the upregulation of CD64, an established marker for the M1 subtype.

The M2c marker CD163 was upregulated in response to the M1 subtype stimulus lipopolysaccharide (LPS). These findings were in line with previous literature, which indicated that macrophages stimulated with interferon-gamma (IFN-γ) or LPS exhibit

increased expression and secretion of pro-inflammatory molecules, representing the classically activated M1 macrophages. The upregulation of the M2a marker CD206 and the M2c marker CD163 was observed during the differentiation of monocytes into macrophages in the presence of IL-4 or IL-10. These findings are also in line with existing literature and support the successful in vitro polarization of monocytes to macrophages for subsequent mass spectrometric imaging (MSI) analysis.

MALDI MSI is a powerful method for the investigation of lipids and metabolites in biological samples without the need for antibody-staining methods. The critical step in MALDI MSI experiments is developing a suitable and reproducible sample preparation method. This study established a comprehensive workflow for the analysis of macrophages, including optimization of sample handling, preparation, measurement, and data analysis. Different macrophage subtypes were cultivated following a widely accepted protocol for differentiating human monocytes. After harvesting, the cells were washed to remove the media, concentrated by centrifugation and shock frosted with liquid nitrogen. Prior to analysis the cell pellets were resolved in PBS. It was found that a spotting volume of 0.2 to 0.5 µL with a concentration of 10,000 cells per µL was sufficient to obtain lipid ion signal intensities in the range of 10,000 counts. Different methods of applying the cell suspensions onto glass slides were compared. Spotting the cells via pipetting resulted in 2 mm diameter spots with an uneven distribution due to the coffee ring effect[94,96,97], which is not ideal for statistical analysis. A pneumatic sprayer achieved a more homogeneous distribution, resulting in more prominent spots (3-4 mm) with improved distribution. This method showed a poorer reproducibility and an increased analysis time leading to the decision to use pipetting for all further experiments. To overcome the issue of spot inhomogeneity, the entire area of a spot was chosen for statistical analysis. The signal intensities for each m/z value were summed up. Besides lipids and peptides, other compounds, such as streptomycin, were detected on the cell spots, indicating residual traces of the medium. Therefore, pure medium control spots were also included for comparison and control.

To test the inter-day reproducibility of the method, *in vitro* differentiated macrophages from the same donor were measured on different days. The MS images showed a homogeneous phospholipid distributions of sphingomyelin $[SM(34:0)+Na]^+$ in all three measurements indicating a good reproducibility. Markers for each macrophage subtype were detected consistently across the measurements. In total, 135 highly significant macrophage markers were identified, demonstrating the reliability and reproducibility of the method.

After optimizing the sample preparation process, three biological replicates were measured in one experiment to identify macrophage subtype-specific markers by MALDI MSI. The medium was spotted in the last row as control. MS images were generated with a 1-100% pixel coverage, and cell-specific distributions were manually filtered. A total number of 3,931 m/z values indicated cell-specific compounds, including various types of adduct ions (Na^+, K^+, NH_4^+) were manually filtered and subjected to statistical analysis using the Perseus software. In total, 145 signals with a p-value smaller than 0.05 were detected. Figures 3a-c display three exemplary macrophage-specific markers. Afterwards, a principal component analysis (PCA) and hierarchical cluster analysis (HCA) were performed on the identified 145 m/z values (see figures 3d-e). Both analyses clearly distinguished the differentiated macrophage

subtypes and revealed a similarity between the anti-inflammatory M2 subtypes, distinct from the pro-inflammatory M1 subtype. Since the majority of the observed 145 m/z values could not be identified using existing databases, it can be assumed that these are modified lipids.

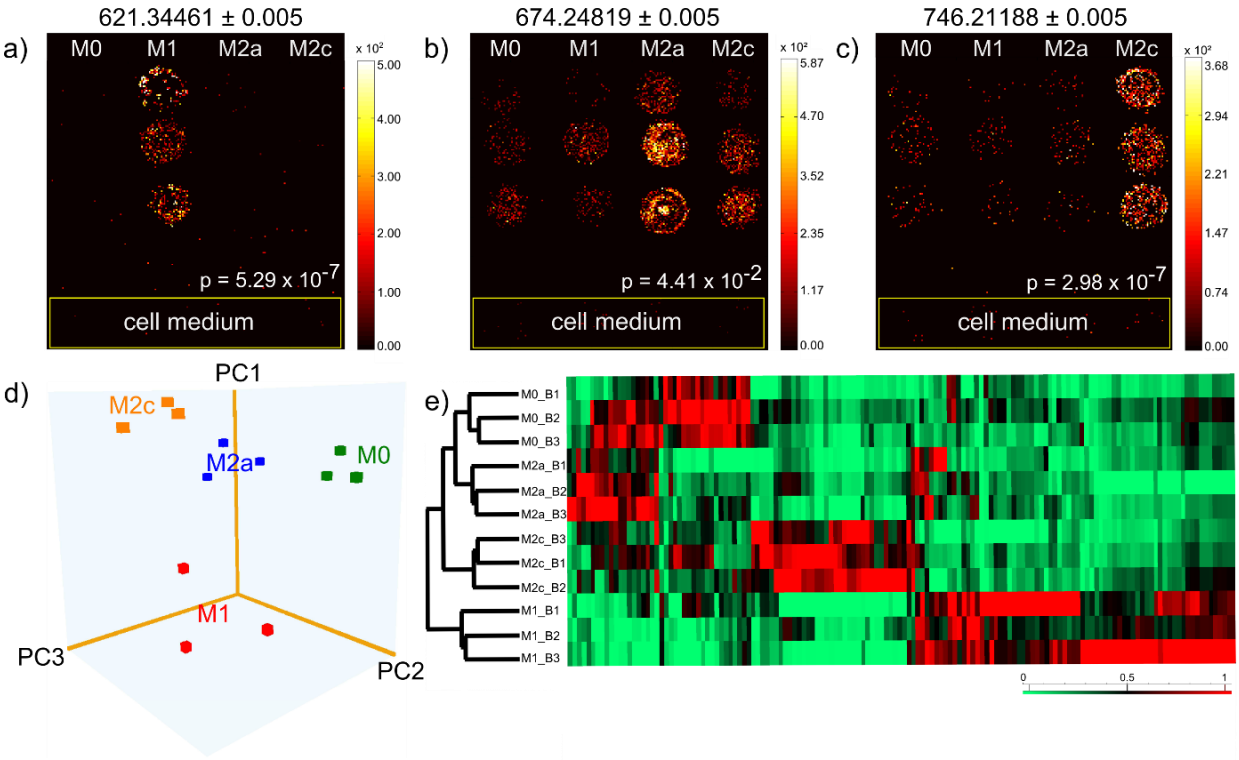

Figure 3: MS images of macrophage-specific markers. (a) m/z 621.34461, (b) m/z 674.24819 and (c) m/z 746.21188. (d) PCA analysis of 145 compounds and compound adducts showing a clear separation between the different macrophage subtypes. (e) Hierarchical clustering analysis (HCA) of the 145 compounds showing the differences between the M1 and M2 subtypes. This figure was taken from the paper published by Khamehgir-Silz et al[95].

To validate the findings, another series of experiments using macrophages from three different donors was conducted with identical experimental parameters. Two markers that were specific to the macrophage types M2c and M1 were consistent in the results, while two other markers were not found in the second set of duplicates, and one marker had a different specificity. The evaluation of the individual dataset verified that there was not a significant shift between the experiments. Statistical analysis was performed using Perseus on both experiments (n=6) with 3,931 m/z values. In total a number of 132 m/z values were identified with a p-value ≤ 0.05. However, only two m/z values consistently showed high signal intensity for a specific macrophage type. These results highlight that a p-value less than 0,05 does not guarantee universal significance but that exact experimental setup or individual sample characteristics may influence the metabolic behavior. The 3D PCA plot of all six biological replicates showed no clear separation between the different macrophage subtypes, indicating the significant heterogeneity of cells derived from different donors. Based on the collected data it remains challenging to defining universal markers for in-vitro stimulated macrophage cell types due to the metabolic heterogeneity between cells isolated from different donors using MALDI-MSI.

A comprehensive workflow for the analysis of human cells was developed, including the determination of cell purity, defining markers based on mRNA and protein expression profiles, and a protocol for MALDI MSI. The results obtained from three biological replicates were in line with previous findings in the literature. However, when the experiment was repeated with three additional donors, the heterogeneity of monocytes derived from different donors, prevented the identification of universal markers on the metabolic level for all cell types. This emphasizes the importance for a guidance on the minimum number of samples to be measured in cell type analysis and the definition of additional measures to ensure reproducibility. In total, the result demonstrate that MALDI MSI is a valuable tool for detecting cell heterogeneity on the metabolic level and easily identifying markers for cell type differentiation. Although MALDI MSI may have lower signal intensities than LC-MS analysis, it offers the advantage of directly using the dataset for tissue imaging experiments without encountering non-matching signals resulting from different ionization techniques.

1.3 Comparative lipid profiling of murine and human atherosclerotic plaques using high-resolution MALDI MSI – (Publication 2 of the cumulative dissertation)[98]

In atherosclerosis, recent studies have utilized MALDI MSI to visualize plaque localization in atherosclerotic mouse models and to evaluate treatment effects on plaque formation and lipid components. Animal studies have identified lipid markers to deepen the understanding of plaque progression[92]. Several studies have examined human samples to explore the potential of imaging lipid biochemistry in human atherosclerosis[87]. However, a direct comparison of murine and human atherosclerotic plaques and the identification of lipid markers for differentiation between ApoE−/− mice and wild-type mice, as well as for human atherosclerotic tissue with differences in progression and medication, have not been extensively performed. The Apolipoprotein E knockout mice (ApoE−/− mice), which is commonly used for the exploration of atherosclerosis, is a genetically altered mouse lacking the Apolipoprotein E gene, consequently causing a subsequent accumulation of cholesterol ester-enriched particles in the blood and promoting the development of atherosclerotic plaques.

This study employed MALDI MSI as a label-free and non-targeted method to address these gaps and determine lipid markers for murine and human atherosclerotic plaques. Young and old male ApoE−/− mice (n=4) and wild-type (WT; n=2) control littermates were used for immunofluorescence analysis and MALDI MS imaging. Human tissue samples were obtained from the National Center for Tumor Diseases (NCT) tissue bank in Heidelberg, Germany. This study measured and analyzed the samples of eight patients with documented atherosclerotic alterations (mean age 63 ± 14.8 years) and three control subjects (mean age 63 ± 5.4 years) without atherosclerotic changes.

Longitudinal or cross cryosections of the murine aorta or carotid artery with a thickness of 10 µm were analyzed using immunofluorescence. The sections were first incubated with a blocking buffer, and then, primary antibodies against the endothelial cell marker CD31 and the monocyte/macrophage marker F4/80 were applied. Subsequently, corresponding secondary antibodies (donkey anti-rat AlexaFluor 488 and donkey anti-rat Dylight 549) were used. Additional staining was performed for MAC387 immunopositive infiltrating macrophages. Cell nuclei were stained with DAPI. The

identification of atherosclerotic plaques was done by staining them with hematoxylin and eosin (H&E) or using Movat's pentachrome staining kit.

All tissue samples were embedded in a metal mold using 5% gelatin to facilitate sectioning for MALDI MSI analysis. Cryosections with a thickness of 10 µm were cut and stored at -80 °C until analysis. Before analysis, the tissue sections were defrosted in a desiccator and covered with a solution of 2,5-dihydroxybenzoic acid (30 mg/mL in acetone:water (1:1) with 0.1% TFA) using an ultrafine matrix preparation sprayer. Afterwards, the samples were analyzed using an atmospheric-pressure MALDI imaging ion source coupled to an orbital trapping mass spectrometer. The measurements were conducted in positive-ion mode with 30 laser pulses per pixel. The mass range covered was from m/z 300 to 1200, and the mass resolution was set to R = 140,000 or R = 240,000 @ m/z 200. Internal mass calibration was performed for improved accuracy. The murine samples were measured with a spatial resolution of 7 µm, while human tissue samples were measured in a spatial resolution range of 5 and 15 µm per pixel, depending on sample size. The characterization of lipids on tissue using MS^2 was unsuccessful due to low signal intensities of the detected markers.

Based on their known role in atherosclerosis plaque development, the following lipid classes were selected for this study: cholesterol esters (CE), lysophosphatidylcholines (LPC), lysophosphatidylethanolamines (LPE), and cholesterol derivatives (CD). However, the MALDI MSI data generated in the study contained additional lipid classes and smaller metabolites that were not explicitly investigated. A total number of 551 lipid species was compiled from the LIPID MAPS database, and their exact mass-to-charge-number ratio (m/z) were calculated using different adducts (H^+, Na^+, K^+, and NH_4^+). Mass spectrometry images were generated with a bin width of Δ(m/z) 0.01 and those images showing a characteristic plaque distribution pattern at aortic bifurcations were chosen for further analysis. Potential markers were selected based on their presence in all samples of >40-week-old ApoE−/− mice and their absence in wild-type (WT) control samples. Mass errors of the potential markers were calculated, and signals with a mass error of less than 3 ppm were retained. The same approach was applied to the human tissue samples, considering the variability in lipid composition. In addition, a list of oxidized lipid species was compiled from the literature. Only two specific oxidized lipids were found in the measured dataset and excluded from the principal component analysis (PCA). For PCA analysis of the murine tissue samples, the intensities of potential markers were exported and normalized to the total ion count (TIC) of each measurement by using the Perseus software. The nonparametric Kruskal-Wallis test was used to determine significant differences in intensity means.

The measurements on murine tissue samples (ApoE−/− and WT) were conducted under the same conditions, making the MALDI-MSI data semi-quantitative. In contrast to the murine samples, the human tissue samples were measured with different spatial resolutions. For the statistical analysis (PCA) and better comparison, the intensities of the detected lipids were assigned to values of 1, 0.5, or 0 for depending on their intensity levels and detection status. The human tissue samples were divided into two groups (atherosclerotic tissue and control). Only lipids fulfilling a prerequisite of 70% of the samples in one group having a value greater than zero were subjected to PCA. The p-values were calculated similarly to the mouse data to assess statistical significance.

In the plaque tissue of older ApoE−/− mice, 65 compounds, including adducts, were identified from the compiled lipid list. Among these compounds, 31 were exclusively found in ApoE−/− mice and not wild-type (WT) mice. The number of detected cholesterol esters in the plaque tissue of older ApoE−/− mice was significantly higher (4.8-fold) than in WT mice and twofold higher than in young ApoE−/− mice. The number of lysophosphatidylcholine (LPC) and lysophosphatidylethanolamine (LPE) lipids, which were the most abundant lipids detected and known to be involved in the development and progression of atherosclerosis, was 1.5-fold higher in the plaque tissue of older ApoE−/− mice compared to WT or young ApoE−/− mice. Specific examples of lipids enriched in the aortic branch and carotid artery of older ApoE−/− mice were identified. For instance, oxysterol 7-ketocholesterol, known to have more potent pro-atherogenic effects than cholesterol, was exclusively detected in lipid-rich plaque regions in arteries branching off the aortic arch. Lysophosphatidylethanolamine LPE(22:0) was mainly detected in the plaque area of the brachiocephalic artery. At the same time, lysophosphatidylcholine LPC(18:2) showed the highest intensity in the plaque located at the root of the brachiocephalic artery and in the vessel wall. The oxidized lipid 9(S)-HODE CE is the stable oxidation product of linoleic acid in CE which contributes to atherosclerosis progression, leading to a fragile, acellular plaque and an increased risk of clinical events detected in the plaque regions.

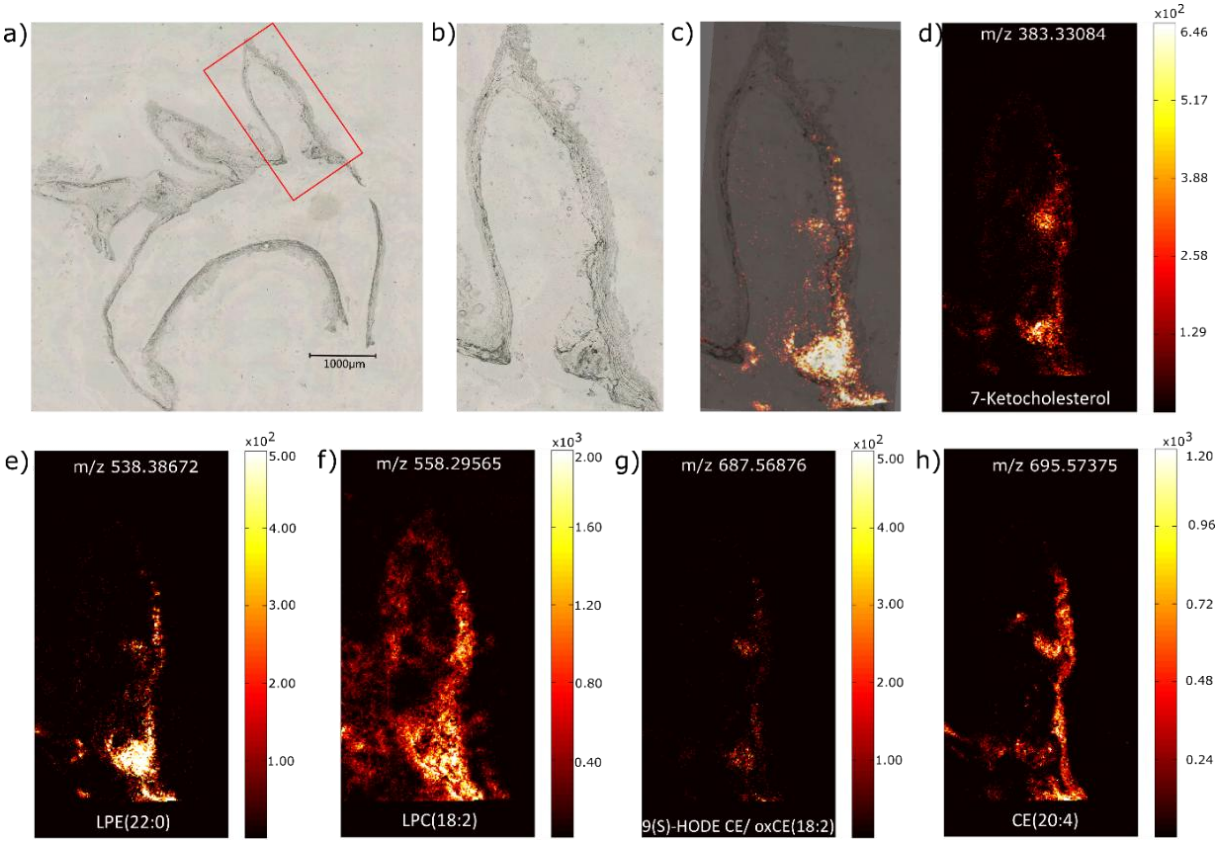

Figure 4: MS imaging of atherosclerotic plaques in the aorta and its branches of ApoE mice. ***a*** *Exemplary brightfield microscopy overview image of a cross-section of the aortic arch and its branches of an old ApoE knockout mouse (ApoE3, 49 weeks). The red square marks the left subclavian artery, which is shown enlarged in* ***b****.* ***c*** *Overlay of the optical image (****b****) and an MS image representing LPE(22:0).* ***d-h*** *MS images of the MALDI MSI measurement in positive-ion mode (pixel size 7 µm, 200 × 400 pixels), presenting examples of different lipids. This figure was taken and adapted from the paper published by Khamehgir-Silz et al*[98]*.*

Interestingly, the cholesterol ester CE(20:4) was not increased in the core plaque area but accumulated in the vessel wall near sites with low or oscillatory shear stress, typically found near the branch point and distal to the plaque.

Statistical analysis of the lipid intensities normalized to the total ion count (TIC) in arterial sections demonstrated significantly higher intensities in the analyzed plaque area of older ApoE−/− mice compared to wild-type and young ApoE−/− mice. The MSI data's principal component analysis (PCA) showed a separation between older ApoE−/− mice, young ApoE−/− mice, and age-matched wild-type mice, indicating distinct lipid compositions within the plaque areas. Overall, the lipid composition within the plaque areas of young ApoE−/− mice was mainly comparable to that of wild-type mice. As the ApoE−/− mice age, an increase in the severity of hypercholesterolemia (high cholesterol levels in the blood) and plasma CE (cholesterol ester) levels have been observed. These changes play a crucial role in the development of atherosclerosis in this murine model. Increased cholesterol and cholesterol ester levels alter the cellular lipid composition, which has been associated with the development of impaired skin barrier function, as described in a recent study [99]. This results suggests that the alterations in lipid composition contribute not only to atherosclerosis but also to other pathological changes in these mice as they age.

The results obtained from human tissue measurements revealed a more diverse distribution of lipids than the murine data. Twenty-six markers exclusively identified in the vessel wall of older ApoE−/− mice were also detected in some human atherosclerotic plaque samples. Eight markers, including cholesterol esters and lysophospholipids, were also found in human control samples. Markers such as cholesterol ester (18:2) and lysophosphatidylcholine (18:2), exclusively found in the arterial specimens of older ApoE−/− mice, were also detected in human control samples. Interestingly, high intensities of cholesteryl acetate and lysolipids LPE(18:0)/LPC(16:1) were found in macrophage-rich regions of the human atherosclerotic vessel wall.

In an extensive data analysis without preselecting markers based on mouse data, a total of 317 m/z values were detected in all human tissue samples and subjected to supervised principal component analysis. The samples were divided into an atherosclerotic artery group and a control group with no significant pathological findings. The list of 317 substances with different m/z values was reduced based on the prerequisite that signals must be detected in at least 70% of the samples in at least one group. PCA of the remaining 25 signals showed a clear separation between the control and atherosclerotic tissue samples. Seven of these detected substances were considered statistically significant atherosclerotic tissue markers, and one species showed a trend towards significance. Among these markers, lysophosphatidylcholine species LPC(22:5) and LPC(22:6) already identified as markers for older atherosclerotic ApoE−/− mice were also identified as markers of human atherosclerotic tissue. These LPCs are products of the phospholipase A2 (PLA2) enzyme activity. High levels of lysophospholipids, such as LPCs, can destabilize membranes. Lipoprotein-associated PLA2 levels have been associated with stroke and atherosclerosis.

Additionally, four glucosylated cholesterol species (16:0, 16:3, 18:3, and 22:0), not detected in murine atherosclerotic tissue, were identified as statistically significant markers for human atherosclerotic plaques. These sterol derivatives belong to the group of sterol lipids and have not been previously described in the context of atherosclerosis. Acetylated cholesteryl glucosides are part of the complex group of glycolipids or steryl glycosides commonly found in plant phytosterol lipids. However, they have recently been discovered in human tissues as storage forms of sterols and contribute to the physical stability of cell membranes. Interestingly, acyl steryl glucosides have been found to stimulate macrophages. The enzymes involved in the biosynthesis of steryl acyl glucosides require exogenous acyl lipids, such as glycerophospholipids, as fatty acid sources for acylation which could explain the observed high content of lysophospholipids, which destabilize cellular membranes. In the study cholesterylsteryl acyl glucosides were predominantly detected in human atherosclerotic tissue but not in the mouse model tissues. It is important to note that higher levels of glycated lipids, such as advanced glycation end products (AGEs), were associated with a plaque rupture phenotype, typically not observed in mouse models.

Furthermore, a notable difference was observed in the lipid composition of patients receiving lipid-lowering drugs compared to those without such medication. The tissue samples of patients receiving an HMG-CoA reductase inhibitor, commonly known as statins, showed significantly lower amounts of cholesterol derivatives (CDs) like oxysterols due to the cholesterol-lowering effect of the medication. Oxysterols, oxidized forms of cholesterol, play a significant role in developing atherosclerotic lesions. They are major constituents of oxidized low-density lipoprotein (oxLDL) and contribute to the accumulation of cholesterol in foam cells derived from macrophages or vascular smooth muscle cells. These foam cells are involved in the formation of atherosclerotic plaques.

This finding indicates that human vascular specimens have a more diverse and patient-dependent distribution of lipids, which differs from the vascular samples derived from the monogenetic ApoE−/− mice. However, it confirms previous research showing that clinically relevant atherosclerotic plaques contain a variable mix of lipids. These lipid profile variations could be related to the different stages of atherosclerosis. Factors such as diet, lifestyle (e.g., a diet rich in fat and sugar, smoking), and medication with cholesterol-lowering drugs can additionally influence the lipid profile and thereby affect the outcome of lipid analysis in atherosclerosis studies.

1.4 Conclusion

This PhD thesis focused on the visualization and characterization of pro-inflammatory and anti-inflammatory human macrophages and atherosclerotic plaques in murine models and human tissue samples using MALDI MSI as a method of choice. The first paper presents a detailed methodology for distinguishing pro-inflammatory and anti-inflammatory human macrophages using MALDI-MSI, RT-qPCR, and FACS. The study successfully differentiated macrophage subtypes M1, M2a, and M2c based on marker gene expression profiles by establishing a comprehensive workflow for sample preparation, measurement, and data analysis in MALDI-MSI experiments. The method showed a good reproducibility and identified subtype-specific markers based on PCA and HCA. The identification of universal markers remains challenging due to the

heterogeneity of human cells deriving from different donors with differences in age, gender, diet and lifestyle.

In the second paper, the lipid composition of murine and human tissue samples was studied. Lipid marker associated with plaque formation and progression in ApoE−/− mice were identified and their presence in human atherosclerotic tissue was studied. The results show significant differences in the lipid composition of older ApoE−/− mice compared to the wild-type mice. The human samples revealed a more heterogeneous distribution of lipids, with some markers overlapping with those identified in murine plaque samples. The results show a patient-dependent distribution of lipids in human vascular specimens, which differ from the monogenetic ApoE−/− mouse model and which is in line with previous publications suggesting that clinically relevant atherosclerotic plaques contain a variable mixture of lipids. The detected variance in lipid compositions could be related to different stages of atherosclerosis progression, diet, lifestyle and medication. This underlines the importance of considering individual patient characteristics (gender, age, diet, medication, etc.) in atherosclerosis studies. Further investigation is required to broaden and validate these findings.

This PhD thesis contributes to the understanding of lipid composition in the context of atherosclerosis and highlights the potential of MALDI MSI as a powerful tool for studying and visualizing the lipid biochemistry in macrophages, murine models and human samples. The results provide valuable insights for future research and may contribute to developing novel diagnostic and therapeutic approaches for cardiovascular diseases.

1.5 Perspectives

This doctoral thesis represents a significant contribution to our understanding of the mechanisms underlying the development of atherosclerosis. Atherosclerosis is a complex and multifaceted inflammatory disease and has been a subject of intense research due to its profound impact on cardiovascular health.This thesis highlights significant aspects of atherosclerotic marker identification by thorough experimentation and rigorous research, aiding in our understanding of the development and progression of plaques[100].

The presented, MSI-based approach was carried out using state of the art technology. Combination of the AP-SMALDI ion source with down to 5 µm routine pixel size and an orbital trapping mass spectrometer takes advantage of both high lateral resolution and high mass spectrometric resolution. The recorded data therefore provides a high density of information regarding the location of hundreds of analytes throughout the samples. The analysis of this huge amount of spectral information is not a trivial task and needs dedicated software solutions. Several tools specialized for signal annotation and identification as well as statistical and network analysis have emerged in the last years. Data from mass spectrometry experiments can be analyzed using the web-based platform Metaspace[101–105]. Metaspace is a platform for metabolite annotation of imaging mass spectrometry data and has integrated machine learning to improve the accuracy and efficiency of identifying molecules within complex mass spectrometry data. By using the isotopic pattern and intensity ratio analysis, researchers can gain deeper insights into the composition and structure of molecules within biological samples. The markers identified in this manner can be subjected to GNPS, a web-

based mass spectrometry ecosystem designed to serve as an open-access knowledge repository for the collaborative organization and sharing of raw, processed, or annotated fragmentation mass spectrometry data (MS/MS) across the research community[106].

An approach to investigate the complexity and diversity of atherosclerosis and to meet the challenges of the microenvironmental plasticity of immune/inflammatory cells is the use of organoids. Organoids are cells derived from inducing and culturing pluripotent stem cells (iPSCs), embryonic stem cells (ESCs), adult stem cells (ASCs) or tumor cells from healthy donors or patients that are incubated under 3D culture systems to aggregate by adhesion, self-organize, and differentiate into 3D cell masses with the corresponding organ tissue morphology[107]. They have a high degree of similarity to their parental cells, replicating and simulating their unique biological characteristics and have the advantage to be analyzed in a controlled biochemical environment.

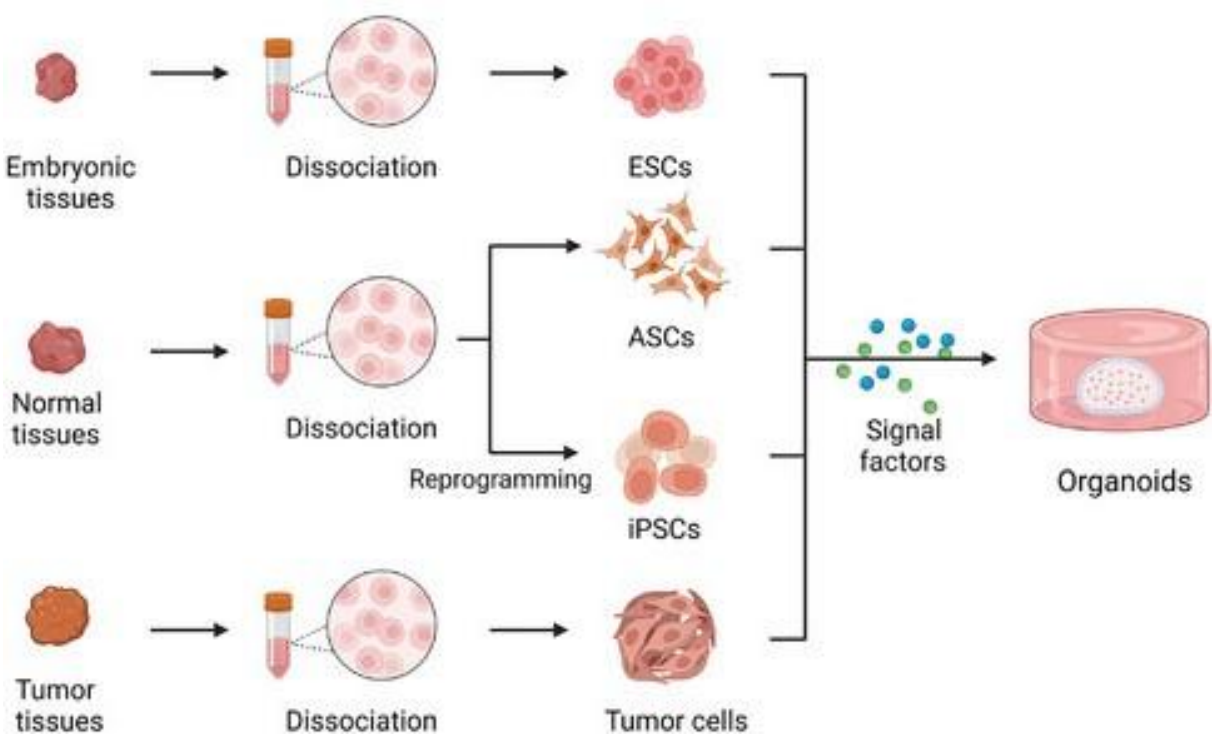

Figure 5:Strategies for in-vitro formation of organoids.This figure was taken and adapted from the paper published by Yang et al.[107]

Organoids have been a subject of research since 1907, when Wilson et al.[108] cultivated mechanically dissociated sponge cells to form functional organisms under in vitro conditions[109]. Since then, organoid research has mainly focused on the isolation and reorganization of cells. In the 1980s, the first pluripotent stem cells (PSCs) were isolated from mouse embryos and obtained by humans, followed by mesenchymal stem cells (MSCs), human embryonic stem cells (ESCs), and induced PSCs (iPSCs)[110]. A study published in 2009 cultured intestinal adult stem cells (ASCs) in vitro to form small intestinal organoids with a crypt-villi structure[111]. This study demonstrates the potential of stem cells to differentiate into spatial structures similar to *in-vivo* organs. Since then the number of research articles reporting of organoids derived from various organs has been increased dramatically[112,113,122–126,114–121]. Also the number of research articles using MSI as analytical tool for the investigation of organoids has

increased since 2000[127]. This rapidly evolving field has already shown promising results by analyzing the presence and spatial distribution of metabolites, lipids, proteins, and drugs within organoids. This approach offers insights into the composition and organization of organoids during development, differentiation, and disease modeling[128] and has been successfully applied to provide a better pathophysiological insight, such as looking into the tumor microenvironment in an organoid model for colorectal cancer[127] or salivary carcinoma[127]. Organoids can also be used to assess the drug response and metabolism by visualizing the distribution and metabolism of drugs within the 3D structure of organoids helping to deepen the understanding of drug uptake, distribution, and metabolic pathways[129]. Another interesting application field of organoids facilitated by MSI, is the biomarker discovery. Analyzing organoids using MSI as method of choice can help to identify potential biomarkers[127] to understand the underlying mechanism of particular disease and can be utilized for diagnostic or therapeutic purposes.

Platforms such as Metaspace and in-vitro model like organoids could be employed to identify markers, make metabolic networks more easily interpretable and help to improve our understanding of the underlying mechanisms of atherosclerosis development and progression, aiding the advancement of novel treatments to reduce or prevent the progression of atherosclerotic plaques.

References

1. Cardiovascular diseases (CVDs). https://www.who.int/news-room/fact-sheets/detail/cardiovascular-diseases-(cvds) (2021).

2. Ilhan, F. & Kalkanli, S. T. Atherosclerosis and the role of immune cells. *World J. Clin. cases* **3**, 345–352 (2015).

3. Gerhardt, T. & Ley, K. Monocyte trafficking across the vessel wall. *Cardiovasc. Res.* **107**, 321–330 (2015).

4. Randolph, G. J. Mechanisms that regulate macrophage burden in atherosclerosis. *Circ. Res.* **114**, 1757–1771 (2014).

5. Liao, J. K. Linking endothelial dysfunction with endothelial cell activation. *J. Clin. Invest.* **123**, 540–541 (2013).

6. Toledo-Pereyra, L. H., Lopez-Neblina, F., Reuben, J. S., Toledo, A. H. & Ward, P. A. Selectin inhibition modulates Akt/MAPK signaling and chemokine expression after liver ischemia-reperfusion. *J. Investig. Surg. Off. J. Acad. Surg. Res.* **17**, 303–313 (2004).

7. Vita, J. A. *et al.* Coronary vasomotor response to acetylcholine relates to risk factors for coronary artery disease. *Circulation* **81**, 491–497 (1990).

8. John, S. *et al.* Increased bioavailability of nitric oxide after lipid-lowering therapy in hypercholesterolemic patients: a randomized, placebo-controlled, double-blind study. *Circulation* **98**, 211–216 (1998).

9. Schächinger, V. *et al.* A positive family history of premature coronary artery disease is associated with impaired endothelium-dependent coronary blood flow regulation. *Circulation* **100**, 1502–1508 (1999).

10. Tacke, F. *et al.* Monocyte subsets differentially employ CCR2, CCR5, and CX3CR1 to accumulate within atherosclerotic plaques. *J. Clin. Invest.* **117**, 185–194 (2007).

11. Tabas, I. & Bornfeldt, K. E. Macrophage Phenotype and Function in Different Stages of Atherosclerosis. *Circ. Res.* **118**, 653–667 (2016).

12. Ley, K., Miller, Y. I. & Hedrick, C. C. Monocyte and macrophage dynamics during atherogenesis. *Arterioscler. Thromb. Vasc. Biol.* **31**, 1506–1516 (2011).

13. Martinez, F. O. & Gordon, S. The M1 and M2 paradigm of macrophage activation: time for reassessment. *F1000Prime Rep.* **6**, 13 (2014).

14. Murray, P. J. *et al.* Macrophage Activation and Polarization: Nomenclature and Experimental Guidelines. *Immunity* **41**, 14–20 (2014).

15. Colin, S., Chinetti-Gbaguidi, G. & Staels, B. Macrophage phenotypes in atherosclerosis. *Immunol. Rev.* **262**, 153–166 (2014).

16. Garg, R., Aggarwal, S., Kumar, R. & Sharma, G. Association of atherosclerosis with dyslipidemia and co-morbid conditions: A descriptive study. *J. Nat. Sci. Biol. Med.* **6**, 163–168 (2015).

17. Wengrofsky, P., Lee, J. & Makaryus, A. N. Dyslipidemia and Its Role in the Pathogenesis of Atherosclerotic Cardiovascular Disease: Implications for Evaluation and Targets for Treatment of Dyslipidemia Based on Recent Guidelines. in (ed. McFarlane, S. I.) Ch. 2 (IntechOpen, 2019). doi:10.5772/intechopen.85772.

18. Poznyak, A. *et al.* The Diabetes Mellitus–Atherosclerosis Connection: The Role of Lipid and Glucose Metabolism and Chronic Inflammation. *International Journal of Molecular Sciences* vol. 21 (2020).

19. Gordon, S. & Taylor, P. R. Monocyte and macrophage heterogeneity. *Nat. Rev. Immunol.* **5**, 953–964 (2005).

20. Martinez, F. O., Helming, L. & Gordon, S. Alternative activation of macrophages: An immunologic functional perspective. *Annu. Rev. Immunol.* **27**, 451–483 (2009).

21. Mosser, D. M. & Edwards, J. P. Exploring the full spectrum of macrophage activation. *Nat. Rev. Immunol.* **8**, 958–969 (2008).

22. Ramprasad, M. P., Terpstra, V., Kondratenko, N., Quehenberger, O. & Steinberg, D. Cell surface expression of mouse macrosialin and human CD68 and their role as macrophage receptors for oxidized low density lipoprotein. *Proc. Natl. Acad. Sci. U. S. A.* **93**, 14833–14838 (1996).

23. Gordon, S. & Martinez, F. O. Alternative activation of macrophages: Mechanism and functions. *Immunity* **32**, 593–604 (2010).

24. Mantovani, A. *et al.* The chemokine system in diverse forms of macrophage activation and polarization. *Trends Immunol.* **25**, 677–686 (2004).

25. Hulka, B. S. & Wilcosky, T. Biological markers in epidemiologic research. *Arch. Environ. Health* **43**, 83–89 (1988).

26. FDA-NIH Biomarker Working Group. BEST (Biomarkers, EndpointS, and other Tools) Resource. www.ncbi.nlm.nih.gov/books/NBK326791/ (2016).

27. Mayeux, R. Biomarkers: potential uses and limitations. *NeuroRx* **1**, 182–188 (2004).

28. Seeley, E. H. & Caprioli, R. M. MALDI imaging mass spectrometry of human tissue: method challenges and clinical perspectives. *Trends Biotechnol.* **29**, 136–143 (2011).

29. Garcia y Narvaiza, D., Navarrete, M. A. H., Falzoni, R., Maier, C. M. & Nazário, A. C. P. Effect of combined oral contraceptives on breast epithelial proliferation in young women. *Breast J.* **14**, 450–455 (2008).

30. Sun, J., Schnackenberg, L. K. & Beger, R. D. Studies of acetaminophen and metabolites in urine and their correlations with toxicity using metabolomics. *Drug Metab. Lett.* **3**, 130–136 (2009).

31. Jansson, J. *et al.* Metabolomics Reveals Metabolic Biomarkers of Crohn's Disease. *PLoS One* **4**, e6386 (2009).

32. Tannahill, G. M. *et al.* Succinate is an inflammatory signal that induces IL-1β through HIF-1α. *Nature* **496**, 238–242 (2013).

33. Abuawad, A., Mbadugha, C., Ghaemmaghami, A. M. & Kim, D.-H. Metabolic characterisation of THP-1 macrophage polarisation using LC–MS-based metabolite profiling. *Metabolomics* **16**, 33 (2020).

34. Zhang, C. *et al.* Quantitative profiling of glycerophospholipids during mouse and human macrophage differentiation using targeted mass spectrometry. *Sci. Rep.* **7**, 412 (2017).

35. Strittmatter, N. *et al.* Analysis of intact bacteria using rapid evaporative ionisation mass spectrometry. *Chem. Commun.* **49**, 6188–6190 (2013).

36. Eroles, M. *et al.* Coupled mechanical mapping and interference contrast

microscopy reveal viscoelastic and adhesion hallmarks of monocyte differentiation into macrophages. *Nanoscale* **15**, 12255–12269 (2023).

37. Spengler, B. Mass spectrometry imaging of biomolecular information. *Anal. Chem.* **87**, 64–82 (2015).

38. Andersen, C. A. & Hinthorne, J. R. Ion Microprobe Mass Analyzer. *Science (80-.).* **175**, 853–860 (1972).

39. HILLENKAMP, F., UNSöLD, E., KAUFMANN, R. & NITSCHE, R. Laser microprobe mass analysis of organic materials. *Nature* **256**, 119–120 (1975).

40. Spengler, B., Hubert, M. & R., K. MALDI ion imaging with a new scanning UV-laser microprobe. in 1041 (1994).

41. Spengler, B. & Cotter, R. J. Ultraviolet laser desorption/ionization mass spectrometry of proteins above 100,000 daltons by pulsed ion extraction time-of-flight analysis. *Anal. Chem.* **62**, 793–796 (1990).

42. Karas, M., Bachmann, D., Bahr, U. & Hillenkamp, F. Matrix-assisted ultraviolet laser desorption of non-volatile compounds. *Int. J. Mass Spectrom. Ion Process.* **78**, 53–68 (1987).

43. Takáts, Z., Wiseman, J. M., Gologan, B. & Cooks, R. G. Mass spectrometry sampling under ambient conditions with desorption electrospray ionization. *Science (80-.).* **306**, 471–473 (2004).

44. Roach, P. J., Laskin, J. & Laskin, A. Nanospray desorption electrospray ionization: an ambient method for liquid-extraction surface sampling in mass spectrometry. *Analyst* **135**, 2233–2236 (2010).

45. Nemes, P. & Vertes, A. Laser ablation electrospray ionization for atmospheric pressure, in vivo, and imaging mass spectrometry. *Anal. Chem.* **79**, 8098–8106 (2007).

46. Sylvester, P. J. & Jackson, S. E. A Brief History of Laser Ablation Inductively Coupled Plasma Mass Spectrometry (LA–ICP–MS). *Elements* **12**, 307–310 (2016).

47. Dilmetz, B. A. *et al.* Novel technical developments in mass spectrometry imaging in 2020: A mini review. *Anal. Sci. Adv.* **2**, 225–237 (2021).

48. Trim, P. J. & Snel, M. F. Small molecule MALDI MS imaging: Current technologies and future challenges. *Methods* **104**, 127–141 (2016).

49. Lanekoff, I., Stevens, S. L., Stenzel-Poore, M. P. & Laskin, J. Matrix effects in biological mass spectrometry imaging: identification and compensation. *Analyst* **139**, 3528–3532 (2014).

50. Rohner, T. C., Staab, D. & Stoeckli, M. MALDI mass spectrometric imaging of biological tissue sections. *Mech. Ageing Dev.* **126**, 177–185 (2005).

51. Bergman, H.-M., Lundin, E., Andersson, M. & Lanekoff, I. Quantitative mass spectrometry imaging of small-molecule neurotransmitters in rat brain tissue sections using nanospray desorption electrospray ionization. *Analyst* **141**, 3686–3695 (2016).

52. Lanekoff, I. *et al.* Imaging nicotine in rat brain tissue by use of nanospray desorption electrospray ionization mass spectrometry. *Anal. Chem.* **85**, 882–889 (2013).

53. Unsihuay, D., Mesa Sanchez, D. & Laskin, J. Quantitative Mass Spectrometry Imaging of Biological Systems. *Annu. Rev. Phys. Chem.* **72**, 307–329 (2021).

54. Taylor, M. J., Lukowski, J. K. & Anderton, C. R. Spatially Resolved Mass Spectrometry at the Single Cell: Recent Innovations in Proteomics and Metabolomics. *J. Am. Soc. Mass Spectrom.* **32**, 872–894 (2021).

55. Schober, Y., Guenther, S., Spengler, B. & Römpp, A. High-resolution matrix-assisted laser desorption/ionization imaging of tryptic peptides from tissue. *Rapid Commun. Mass Spectrom.* **26**, 1141–1146 (2012).

56. Schober, Y., Schramm, T., Spengler, B. & Römpp, A. Protein identification by accurate mass matrix-assisted laser desorption/ionization imaging of tryptic peptides. *Rapid Commun. Mass Spectrom.* **25**, 2475–2483 (2011).

57. Heijs, B. *et al.* Comprehensive Analysis of the Mouse Brain Proteome Sampled in Mass Spectrometry Imaging. *Anal. Chem.* **87**, 1867–1875 (2015).

58. Rocha, B. *et al.* Characterization of lipidic markers of chondrogenic differentiation using mass spectrometry imaging. *Proteomics* **15**, 702–713 (2015).

59. Römpp, A. & Spengler, B. Mass spectrometry imaging with high resolution in mass and space. *Histochem. Cell Biol.* **139**, 759–783 (2013).

60. Garikapati, V., Karnati, S., Bhandari, D. R., Baumgart-Vogt, E. & Spengler, B. High-resolution atmospheric-pressure MALDI mass spectrometry imaging workflow for lipidomic analysis of late fetal mouse lungs. *Sci. Rep.* **9**, 3192 (2019).

61. Kadesch, P., Quack, T., Gerbig, S., Grevelding, C. G. & Spengler, B. Lipid Topography in Schistosoma mansoni Cryosections, Revealed by Microembedding and High-Resolution Atmospheric-Pressure Matrix-Assisted Laser Desorption/Ionization (MALDI) Mass Spectrometry Imaging. *Anal. Chem.* **91**, 4520–4528 (2019).

62. Huber, K. *et al.* Approaching cellular resolution and reliable identification in mass spectrometry imaging of tryptic peptides. *Anal. Bioanal. Chem.* **410**, 5825–5837 (2018).

63. Norris, J. L. & Caprioli, R. M. Analysis of Tissue Specimens by Matrix-Assisted Laser Desorption/Ionization Imaging Mass Spectrometry in Biological and Clinical Research. *Chem. Rev.* **113**, 2309–2342 (2013).

64. Caprioli, R. M., Farmer, T. B. & Gile, J. Molecular Imaging of Biological Samples: Localization of Peptides and Proteins Using MALDI-TOF MS. *Anal. Chem.* **69**, 4751–4760 (1997).

65. Stoeckli, M., Chaurand, P., Hallahan, D. E. & Caprioli, R. M. Imaging mass spectrometry: A new technology for the analysis of protein expression in mammalian tissues. *Nat. Med.* **7**, 493–496 (2001).

66. Kompauer, M., Heiles, S. & Spengler, B. Atmospheric pressure MALDI mass spectrometry imaging of tissues and cells at 1.4-μm lateral resolution. *Nat. Methods* **14**, 90–96 (2016).

67. Kompauer, M., Heiles, S. & Spengler, B. Autofocusing MALDI mass spectrometry imaging of tissue sections and 3D chemical topography of nonflat surfaces. *Nat. Methods* **14**, 1156–1158 (2017).

68. Lemaire, R. *et al.* Direct Analysis and MALDI Imaging of Formalin-Fixed, Paraffin-Embedded Tissue Sections. *J. Proteome Res.* **6**, 1295–1305 (2007).

69. Wisztorski, M., Franck, J., Salzet, M. & Fournier, I. MALDI Direct Analysis and Imaging of Frozen Versus FFPE Tissues: What Strategy for Which Sample? BT - Mass Spectrometry Imaging: Principles and Protocols. in (eds. Rubakhin, S. S. & Sweedler, J. V) 303–322 (Humana Press, 2010). doi:10.1007/978-1-60761-746-4_18.

70. Karas, M. & Krüger, R. Ion Formation in MALDI: The Cluster Ionization Mechanism. *Chem. Rev.* **103**, 427–440 (2003).

71. Jaskolla, T. W. & Karas, M. Compelling Evidence for Lucky Survivor and Gas Phase Protonation: The Unified MALDI Analyte Protonation Mechanism. *J. Am. Soc. Mass Spectrom.* **22**, 976–988 (2011).

72. Paschke, C. *et al.* Mirion—A Software Package for Automatic Processing of Mass Spectrometric Images. *J. Am. Soc. Mass Spectrom.* **24**, (2013).

73. Robichaud, G., Garrard, K. P., Barry, J. A. & Muddiman, D. C. MSiReader: an open-source interface to view and analyze high resolving power MS imaging files on Matlab platform. *J. Am. Soc. Mass Spectrom.* **24**, 718–721 (2013).

74. Bokhart, M. T., Nazari, M., Garrard, K. P. & Muddiman, D. C. MSiReader v1.0: Evolving Open-Source Mass Spectrometry Imaging Software for Targeted and Untargeted Analyses. *J. Am. Soc. Mass Spectrom.* **29**, 8–16 (2018).

75. Kompauer, M., Heiles, S. & Spengler, B. Atmospheric pressure MALDI mass spectrometry imaging of tissues and cells at 1.4-μm lateral resolution. *Nat. Methods* **14**, 90–96 (2017).

76. Hartler, J. LIPID MAPS: Tools and Databases BT - Encyclopedia of Lipidomics. in (ed. Wenk, M. R.) 1–4 (Springer Netherlands, 2015). doi:10.1007/978-94-007-7864-1_11-1.

77. Sud, M., Fahy, E., Cotter, D., Dennis, E. A. & Subramaniam, S. LIPID MAPS-Nature Lipidomics Gateway: An Online Resource for Students and Educators Interested in Lipids. *J. Chem. Educ.* **89**, 291–292 (2012).

78. Smith, C. A. *et al.* METLIN: A Metabolite Mass Spectral Database. *Ther. Drug Monit.* **27**, (2005).

79. Römpp, A. *et al.* Histology by Mass Spectrometry: Label-Free Tissue

Characterization Obtained from High-Accuracy Bioanalytical Imaging. *Angew. Chemie Int. Ed.* **49**, 3834–3838 (2010).

80. Schwamborn, K. & Caprioli, R. M. Molecular imaging by mass spectrometry — looking beyond classical histology. *Nat. Rev. Cancer* **10**, 639–646 (2010).

81. Müller, M. A., Zweig, N., Spengler, B., Weinert, M. & Heiles, S. Lipid Signatures and Inter-Cellular Heterogeneity of Naïve and Lipopolysaccharide-Stimulated Human Microglia-like Cells. *Anal. Chem.* **95**, 11672–11679 (2023).

82. Lawson, L. J., Perry, V. H., Dri, P. & Gordon, S. Heterogeneity in the distribution and morphology of microglia in the normal adult mouse brain. *Neuroscience* **39**, 151–170 (1990).

83. Lenz, K. M. & McCarthy, M. M. A starring role for microglia in brain sex differences. *Neurosci. a Rev. J. bringing Neurobiol. Neurol. psychiatry* **21**, 306–321 (2015).

84. Butovsky, O. & Weiner, H. L. Microglial signatures and their role in health and disease. *Nat. Rev. Neurosci.* **19**, 622–635 (2018).

85. Li, Q. & Barres, B. A. Microglia and macrophages in brain homeostasis and disease. *Nat. Rev. Immunol.* **18**, 225–242 (2018).

86. Cao, J. *et al.* Atheroma-Specific Lipids in ldlr(-/-) and apoe(-/-) Mice Using 2D and 3D Matrix-Assisted Laser Desorption/Ionization Mass Spectrometry Imaging. *J. Am. Soc. Mass Spectrom.* **31**, 1825–1832 (2020).

87. Visscher, M. *et al.* Data Processing Pipeline for Lipid Profiling of Carotid Atherosclerotic Plaque with Mass Spectrometry Imaging. *J. Am. Soc. Mass Spectrom.* **30**, 1790–1800 (2019).

88. Moerman, A. M. *et al.* Lipid signature of advanced human carotid atherosclerosis assessed by mass spectrometry imaging. *J. Lipid Res.* **62**, (2021).

89. Kaya, I., Sämfors, S., Levin, M., Borén, J. & Fletcher, J. S. Multimodal MALDI Imaging Mass Spectrometry Reveals Spatially Correlated Lipid and Protein Changes in Mouse Heart with Acute Myocardial Infarction. *J. Am. Soc. Mass Spectrom.* **31**, 2133–2142 (2020).

90. Shen, L. *et al.* Identification and visualization of oxidized lipids in atherosclerotic plaques by microscopic imaging mass spectrometry-based metabolomics. *Atherosclerosis* **311**, 1–12 (2020).

91. Lohöfer, F. *et al.* Mass Spectrometry Imaging of atherosclerosis-affine Gadofluorine following Magnetic Resonance Imaging. *Sci. Rep.* **10**, 79 (2020).

92. Castro-Perez, J. *et al.* In vivo isotopically labeled atherosclerotic aorta plaques in ApoE KO mice and molecular profiling by matrix-assisted laser desorption/ionization mass spectrometric imaging . *Rapid Commun. Mass Spectrom.* **28**, 2471–2479 (2014).

93. Greco, F. *et al.* Lipids associated with atherosclerotic plaque instability revealed by mass spectrometry imaging of human carotid arteries. *Atherosclerosis* **397**, 118555 (2024).

94. Greco, F. *et al.* Mass Spectrometry Imaging as a Tool to Investigate Region Specific Lipid Alterations in Symptomatic Human Carotid Atherosclerotic Plaques. *Metabolites* vol. 11 (2021).

95. Khamehgir-Silz, P. *et al.* Strategy for marker-based differentiation of pro- and anti-inflammatory macrophages using matrix-assisted laser desorption/ionization mass spectrometry imaging. *Analyst* **143**, 4273–4282 (2018).

96. Garden, R. W. & Sweedler, J. V. Heterogeneity within MALDI Samples As Revealed by Mass Spectrometric Imaging. *Anal. Chem.* **72**, 30–36 (2000).

97. Deegan, R. D. *et al.* Capillary flow as the cause of ring stains from dried liquid drops. *Nature* **389**, 827–829 (1997).

98. Khamehgir-Silz, P. *et al.* Comparative lipid profiling of murine and human atherosclerotic plaques using high-resolution MALDI MSI. *Pflugers Arch.* **474**, 231–242 (2022).

99. Martins Cardoso, R. *et al.* Hypercholesterolemia in young adult APOE−/− mice alters epidermal lipid composition and impairs barrier function. *Biochim. Biophys. Acta - Mol. Cell Biol. Lipids* **1864**, 976–984 (2019).

100. Worthmann, A. & Bartelt, A. MALDI MSI for a fresh view on atherosclerotic

plaque lipids. *Pflugers Arch.* **474**, 185–186 (2022).

101. Palmer, A. *et al.* FDR-controlled metabolite annotation for high-resolution imaging mass spectrometry. *Nat. Methods* **14**, 57–60 (2016).

102. Ovchinnikova, K., Kovalev, V., Stuart, L. & Alexandrov, T. OffsampleAI: artificial intelligence approach to recognize off-sample mass spectrometry images. *BMC Bioinformatics* **21**, 129 (2020).

103. Ovchinnikova, K., Stuart, L., Rakhlin, A., Nikolenko, S. & Alexandrov, T. ColocML: machine learning quantifies co-localization between mass spectrometry images. *Bioinformatics* **36**, 3215–3224 (2020).

104. Alexandrov, T. *et al.* METASPACE: A community-populated knowledge base of spatial metabolomes in health and disease. *bioRxiv* 539478 (2019) doi:10.1101/539478.

105. Alexandrov, T. Spatial Metabolomics and Imaging Mass Spectrometry in the Age of Artificial Intelligence. *Annu. Rev. Biomed. Data Sci.* **3**, 61–87 (2020).

106. Wang, M. *et al.* Sharing and community curation of mass spectrometry data with Global Natural Products Social Molecular Networking. *Nat. Biotechnol.* **34**, 828–837 (2016).

107. Yang, S. *et al.* Organoids: The current status and biomedical applications. *MedComm* **4**, e274 (2023).

108. Wilson, H. V. A NEW METHOD BY WHICH SPONGES MAY BE ARTIFICIALLY REARED. *Science* **25**, 912–915 (1907).

109. Corrò, C., Novellasdemunt, L. & Li, V. S. W. A brief history of organoids. *Am. J. Physiol. Physiol.* **319**, C151–C165 (2020).

110. Yu, J. *et al.* Induced pluripotent stem cell lines derived from human somatic cells. *Science* **318**, 1917–1920 (2007).

111. Sato, T. *et al.* Single Lgr5 stem cells build crypt-villus structures in vitro without a mesenchymal niche. *Nature* **459**, 262–265 (2009).

112. Huang, L. *et al.* Commitment and oncogene-induced plasticity of human stem cell-derived pancreatic acinar and ductal organoids. *Cell Stem Cell* **28**, 1090-1104.e6 (2021).

113. Randriamanantsoa, S. *et al.* Spatiotemporal dynamics of self-organized branching in pancreas-derived organoids. *Nat. Commun.* **13**, 5219 (2022).

114. Hallett, J. M. *et al.* Human biliary epithelial cells from discarded donor livers rescue bile duct structure and function in a mouse model of biliary disease. *Cell Stem Cell* **29**, 355-371.e10 (2022).

115. Roos, F. J. M. *et al.* Human branching cholangiocyte organoids recapitulate functional bile duct formation. *Cell Stem Cell* **29**, 776-794.e13 (2022).

116. Shinozawa, T. *et al.* High-Fidelity Drug-Induced Liver Injury Screen Using Human Pluripotent Stem Cell–Derived Organoids. *Gastroenterology* **160**, 831-846.e10 (2021).

117. Hendriks, D., Artegiani, B., Hu, H., Chuva de Sousa Lopes, S. & Clevers, H. Establishment of human fetal hepatocyte organoids and CRISPR-Cas9-based gene knockin and knockout in organoid cultures from human liver. *Nat. Protoc.* **16**, 182–217 (2021).

118. Eicher, A. K. *et al.* Functional human gastrointestinal organoids can be engineered from three primary germ layers derived separately from pluripotent stem cells. *Cell Stem Cell* **29**, 36-51.e6 (2022).

119. Song, H. *et al.* Establishment of Patient-Derived Gastric Cancer Organoid Model From Tissue Obtained by Endoscopic Biopsies. *J. Korean Med. Sci.* **37**, e220 (2022).

120. Han, Y. *et al.* Identification of SARS-CoV-2 inhibitors using lung and colonic organoids. *Nature* **589**, 270–275 (2021).

121. Yokota, E. *et al.* Clinical application of a lung cancer organoid (tumoroid) culture system. *NPJ Precis. Oncol.* **5**, 29 (2021).

122. Saha, A. *et al.* Cone photoreceptors in human stem cell-derived retinal organoids demonstrate intrinsic light responses that mimic those of primate fovea. *Cell Stem Cell* **29**, 460-471.e3 (2022).

123. Finkbeiner, C. *et al.* Single-cell ATAC-seq of fetal human retina and stem-cell-derived retinal organoids shows changing chromatin landscapes during cell fate acquisition. *Cell Rep.* **38**, 110294 (2022).

124. Jgamadze, D. *et al.* Structural and functional integration of human forebrain organoids with the injured adult rat visual system. *Cell Stem Cell* **30**, 137-152.e7 (2023).

125. Gupta, N. *et al.* Modeling injury and repair in kidney organoids reveals that homologous recombination governs tubular intrinsic repair. *Sci. Transl. Med.* **14**, eabj4772 (2024).

126. Tran, T. *et al.* A scalable organoid model of human autosomal dominant polycystic kidney disease for disease mechanism and drug discovery. *Cell Stem Cell* **29**, 1083-1101.e7 (2022).

127. Zivko, C. *et al.* Mass Spectrometry Imaging of Organoids to Improve Preclinical Research. *Adv. Healthc. Mater.* **13**, 2302499 (2024).

128. Avelino, T. M. *et al.* Mass spectrometry-based proteomics of 3D cell culture: A useful tool to validate culture of spheroids and organoids. *SLAS Discov. Adv. life Sci. R D* **27**, 167–174 (2022).

129. Spencer, C. E. *et al.* Role of MALDI-MSI in combination with 3D tissue models for early stage efficacy and safety testing of drugs and toxicants. *Expert Rev. Proteomics* **17**, 827–841 (2020).

Table 1: Documentation of the usage of AI tools

AI tool	Form of use	Affected parts of the work	URL
DeepL Translator	1. Translation of literature text passages 2. Grammer checker	1. N/A 2. Whole work	https://www.deepl.com/de/translator; last access 31.03.2025
Scibbr	1. Grammer checker 2. Text correction*	1.Whole work 2.Whole work	https://www.scribbr.de ; last access 31.03.2025
QuillBot	1. Grammer checker 2. Summary of literature text passage 3. Text correction and optimazation of phrasing*	1. Whole work 2. N/A 3. Whole work	https://quillbot.com/; last access 31.03.2025

*The AI tools were used for text correction and optimization of the phrasing. The proposed text was used as a drafting aid and edited

Pegah Khamehgir-Silz, Florian Schnitter, Andreas H. Wagner, Stefanie Gerbig, Sabine Schulz, Markus Hecker and Bernhard Spengler, Strategy for marker-based differentiation of pro- and anti-inflammatory macrophages using matrix-assisted laser desorption/ionization mass spectrometry imaging, Analyst, 2018,143, 4273-4282, https://doi.org/10.1039/C8AN00659H

Pegah Khamehgir-Silz, Stefanie Gerbig, Nadine Volk, Sabine Schulz, Bernhard Spengler, Markus Hecker, Andreas H. Wagner, Comparative lipid profiling of murine and human atherosclerotic plaques using high-resolution MALDI MSI, Pflugers Arch. 2022; 474(2): 231–242, https://doi.org/10.1007/s00424-021-02643-x

Acknowledgements

This thesis would not be possible without the help and support of so many people in so many ways. It was the product of large measures of prospects and furious encounters with people who have changed the course of my academic career.

First and foremost, I would like to thank Prof. Dr. Bernhard Spengler for allowing me to work in his research group and for his scientific supervision of my work. His support and encouragement have guided me through challenges and visualized new perspectives. I am also very grateful to Prof. Dr. Andreas Wagner for his time and willingness to be my second referee for this doctoral thesis.

In addition, I would also like to thank Dr. Sabine Schulz, Dr. Stefanie Gerbig and again Prof. Andreas H. Wagner for scientific supervision and guidance of my work. The advice, assistance, profound knowledge, and practical experience encouraged me to keep going forward.

Thanks to all the group members at the Institute of Inorganic and Analytical Chemistry, who guaranteed an excellent working environment. I always appreciated the strong collaboration.

Finally, I would like to thank my parents, my husband, my children and my brother for their continuous support, patience and encouragement and for their strong belief in my skills.